Turbulence and Coherent Structure Characterisation in a Tidally Energetic Channel

Lucas, Natasha; Austin, Martin; Rippeth, Tom; Powell, Ben; Wakonigg, Pablo

Renewable Energy

DOI:
https://doi.org/10.1016/j.renene.2022.05.044

Published: 01/07/2022

Turbulence and Coherent Structure Characterisation in a Tidally Energetic Channel

Natasha S Lucas[a,*], Martin J Austin[b], Tom P Rippeth[b], Ben Powell[b], Pablo Wakonigg[b]

[a] *British Antarctic Survey, High Cross, Madingley Road, Cambridge, CB3 0ET, UK*
[b] *School of Ocean Sciences, Bangor University, Menai Bridge, Anglesey, LL59 5AB, UK*

Abstract

Understanding the temporal and spatial characteristics of turbulent coherent structures is of interest to the emergent sector of marine renewable energy for power generation from tidal stream turbines as loading due to these vortex structures has resulted in costly device failure. Here methods for characterising these coherent structures are developed using an off the shelf broadband acoustic Doppler current profiler (ADCP) vertical beam with the metrics fast Fourier transforms and a wavelet element model. Results indicate lengthscales fall in the range 2.5 to 51 m. Focused study on a 30-minute window finds the 5 most powerful features have a median lengthscale of 13.2 m and the strongest signal lies at ∼6.8 m, which scale to 0.9 and 0.4 times the water depth respectively, these features have a periodicity of ∼127 s. Methods using variance across ADCP beams are common for turbulence characterisation within the tidal energy sector, with turbulence intensity being appropriated from the wind energy sector. However, turbulence intensity is found to be

*Corresponding author
Email address: nacas@bas.ac.uk (Natasha S Lucas)

a poor predictor water column turbulence in the presence of coherent structures.
Keywords: Hydrodynamics, Tidal stream turbines, Coherent Structures, Tidal Power, Variance Method, Alternative Energy Site Assessment

1. Introduction

Marine renewable electrical power generation using tidal energy turbines offers great potential. However recent failures in deployments are thought likely to be due to turbulent coherent structures in the water column, resulting in variable stresses on turbines, causing gearbox loading from misalignment and costly blade bending [1, 2, 3, 4]. Detailed knowledge acquisition of site specific turbulence characterisation including these intermittent, coherent events is needed for design optimisation of these devices.

Recent tidal energy workshops [5] have highlighted the need to develop a standard method of measuring turbulence and industry standard post-processing data methods, with the suggestion that transfer functions from the wind sector, such as the International Electrotechnical Commission (IEC) standard metric of turbulence intensity (TI) are the way forward. However, turbulence intensity does not capture coherent structure information, with oceanic and atmospheric turbulence differing due to seasonal, tidal and diurnal forcings [6]. Temporal and spatial turbulence information from energetic tidal channels is needed with instrumentation available to the field. For full spatial information, large arrays of instrumentation would be required, but this is cost prohibitive and as such novel metrics that are able to capture higher order statistics giving insight into environmental turbulent signals on many scales would be advantageous.

The tidal turbine sector needs inflow conditions for models, but there are currently gaps in information about ambient turbulent conditions on scales from small chaotic to large scale coherent structures. McCaffrey et al. [6] suggest that timescales and dimensions of turbulent structures are not well represented in such models. Current computational models, such as TurbSim (National Renewable Energy Laboratory (NREL), Washington DC), are not able to model all scales; only simulating basic flow regimes. They use inputs of TI and power spectral density to model spatial coherence and use this to force FAST (NREL) code which requires the 3-D structure of turbulence [7]. Despite these limitations, TI and turbulence spectra from velocity variance are shown to correlate with turbine performance and structural fatigue, with contributions from wakes and ambient turbulence [8, 9].

Lenthscales of coherent turbulent structures in the marine environment are thought likely to be anywhere in the region of $\mathcal{O}1$ m to $\mathcal{O}80$ m [10, 11, 12, 13, 14, 15, 16, 17, 18, 6, 7, 19, 20, 21, 22, 23, 24, 25], with evolution and stretching thought likely as they evolve within the water column [10]. Much work has been done on coherent structure understanding within theoretical and laboratory settings [26, 27, 28, 29, 30, 31, 32, 33, 34, 35], with understanding of vortex formation, deflection angle and structure established.

Vertical and horizontal structure is thought to affect energy balances, with friction, inertia and phase differences resulting in variation of energy dissipated in the system [36, 37] and turbulent kinetic energy asymmetries in flood and ebb tides being common, attributed to upstream bathymetry affecting boundary layer thickness and small-scale intermittency and asymmetries [37, 38, 39]. Coincident measurements of turbulent kinetic energy production and dissipation in tidal channels suggest that the common assumption of a local energy balance does not always apply [40, 4], and this is attributed to advection of energy via these coherent structures and their vorticity fluxes [41, 37], with aerial imagery adding weight to this hypothesis showing advected eddies and associated strong lateral shear [37].

Coherent structures become known as boils when their turbulent signature impinges on the free-surface, transmitting vorticity to a horizontally radial outward current, transporting momentum and often bringing colder, sediment or contaminant enriched water from below [28, 42, 43, 14, 44, 11, 15]. These smooth, short wavelength damped boil patches with, in some cases, a wave ringed edge [45], have typical diameters at the ocean surface of 0.5 to 1.1 h, where h is the water depth [15, 19]. The life-cycle of a coherent structure from formation through to dissipation as a free-surface boil is illustrated in Figure 1.

This work aims to identify measurable metrics for the characterisation of marine turbulent macroscale coherent structures and their temporal and spatial configuration in a tidally energetic channel using a standard Acoustic Doppler Current Profiler (ADCP) correlated with high resolution camera imagery to provide a tool for the tidal energy industry to help predict turbine and blade loading and inform an improved physical description of the flow.

In order to understand the magnitude and scales of temporal and spatial marine turbulence structures, this study will use camera images to capture surface boil occurrence and the vertical beam of an ADCP for direct analysis of flow components using higher-order metrics. These metrics will then be

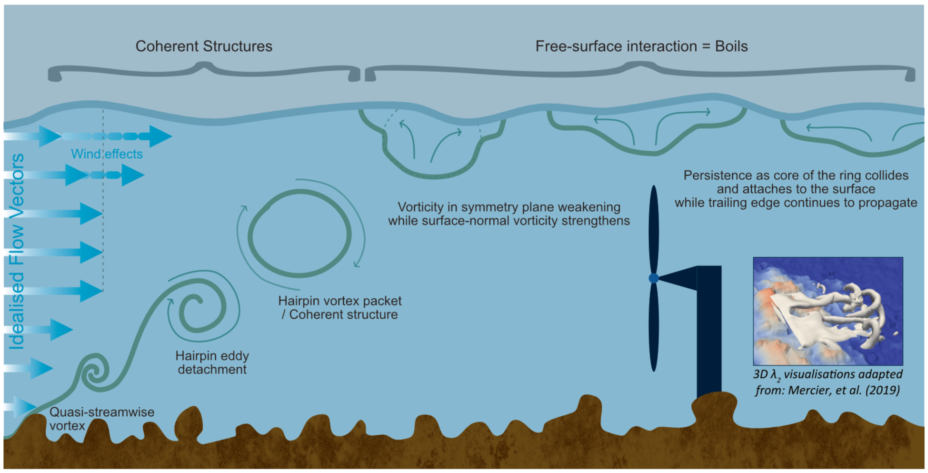

Figure 1: Schematic illustrating the life-cycle of a coherent structure from generation at the sea bed to dissipation at the free-surface. Accompanied by an inlay figure from Mercier et al. [46] showing a simulation of λ_2 isosurface plot of a 10 m wide turbulent coherent flow structure generated at bathymetric elevations.

utilised to asses the implications of the presence of coherent structures on other turbulent benchmarks obtained from modification to the flow components using the Janus configuration beams. Energy production and dissipation within the system will be appraised in this process. Further scrutiny of surface boil properties will be carried out in a subsequent paper; utilising geo-rectified capture of the high resolution camera images at high frequency.

This paper is organised as follows: in Section 2, the study site and instrumentation experimental settings are detailed, followed by methodical details of analytical data processing methods and noise. In Section 3 we examine the experimental outputs with objective presentation of the results from camera capture, fast Fourier transforms and wavelets for temporal and spatial information, and turbulent kinetic energy dissipation and production to observe the energy balances. Section 4 discusses the findings in the context of the tidal energy industry and the implications for identification of measurable metrics for characterisation of marine turbulence in tidal races. Conclusions are given in Section 5, followed by possible future areas for research; Section 6.

2. Methodology

2.1. Study area and instrumentation

Data examined in this study were collected using a Nortek 5-beam Signature 1000 ADCP mounted 0.5 m above the seabed adjacent to Menai Bridge on the western side of the Menai Strait and a high resolution camera monitoring the sea surface mounted to the School of Ocean Sciences building overlooking a portion of the Menai Strait incorporating the ADCP deployment.

The Menai Strait is a ~25 km long stretch of shallow tidal water separating Anglesey from mainland Wales, UK, with width at the study site of ~500 m. This un-stratified tidal channel, with flood direction NE to SW, has a highly energetic modified semi-diurnal tide with maximum spring tide range of ~6 m and depth-mean streamwise tidal velocities in the main channel reaching 2.5 m s^{-1} [47]. The location is sheltered thus the risk of contamination of observations by surface waves is greatly reduced [48, 49].

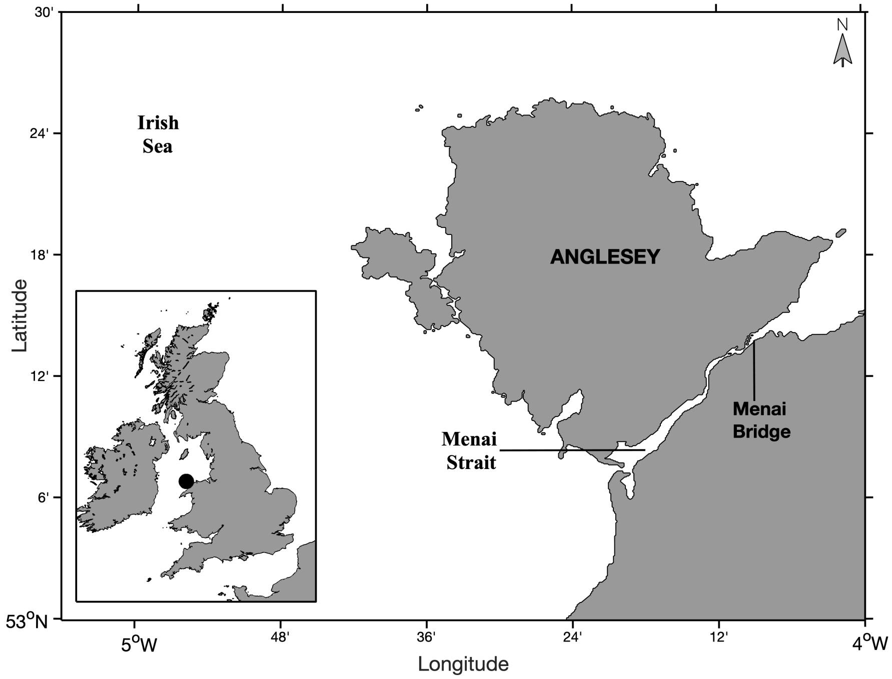

Figure 2: Geographic location map showing the Menai Strait, UK with the ADCP location close to Menai Bridge.

The geographic location is shown in Figure 2. The bathymetry, ADCP and camera location and ADCP orientation is shown in Figure 3. The ADCP was aligned with a tilt and pitch of of 2.7 and 5.4° respectively, with beam 4 sampling primarily along the ADCP current ebb direction, beam 2 along the flood direction, and beams 1 and 3 positioned across the flow. A dive survey characterised the seabed through visual inspection [50] as being mixed sand-gravel with some larger boulders.

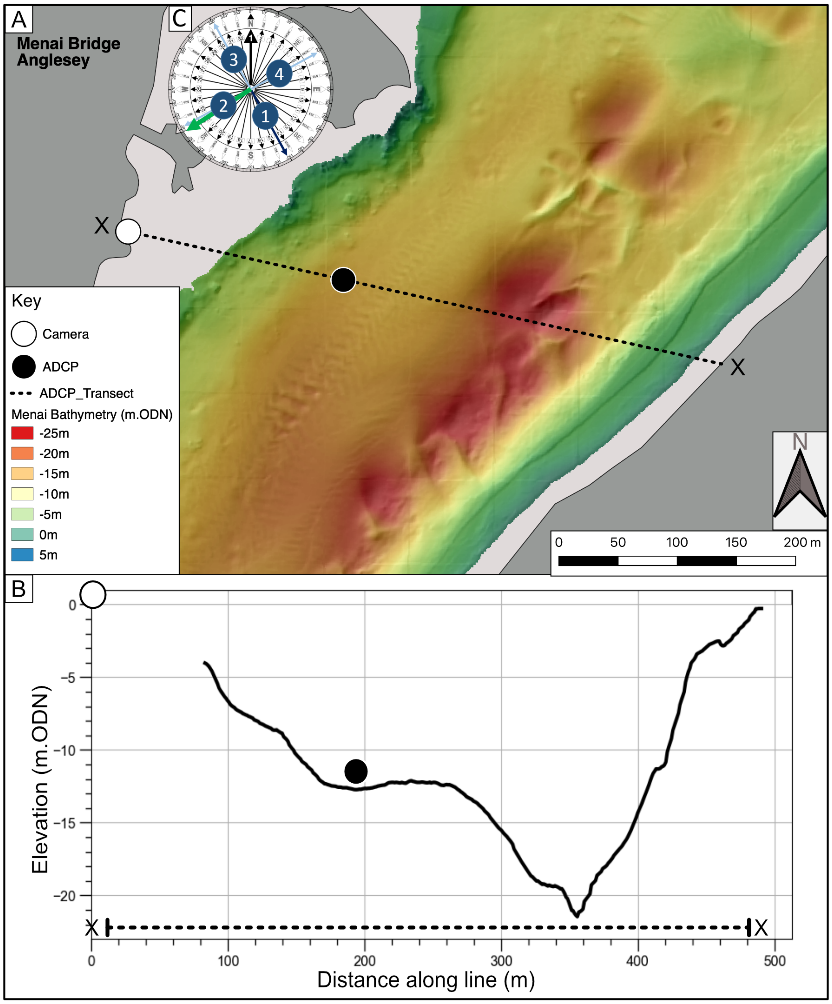

Figure 3: A) Bathymetry map adjacent to Menai Bridge, Anglesey [51], B) Profile of transect X-X showing the deployment positions of the camera and ADCP (53.225519N, 4.157497W), and C) ADCP Transducer orientation (numbers and blue arrows, dark blue being the ADCP heading angle) and mean flow direction during the periods used in the variance analysis (green arrow)

The ADCP was configured firstly to obtain mean flow components using 'Average mode' Earth coordinate data and subsequently to sample continuously giving 'Burst mode' high precision beam line data. All data acquisition had a blanking distance of 0.1 m and due to the sea surface variation over the tidal cycle height above bed (metres above bed: mab) is used as the vertical coordinate system. Prior to analysis, data were quality controlled by removing acoustic surface reflection due to side lobe interference by taking the correlation minima near the surface on a dataset basis. For the 'Average mode' data 8 cells (3.2 m) below the ADCP pressure reading were masked. For the 'Burst mode' data, the correlation minima denoted removing 4 bins (1.2 m). The data were then masked with the recommended 50% correlation cutoff [52]. To improve signal to noise ratio (SNR) data analysis performed using 'Burst' mode were then ensemble averaged to 2 s.

The 'Average mode' mean flow Earth coordinate data was recorded over 38 x 0.4 m cells at 1 ping every 2 seconds for 2 minute bursts, with a 19 minute gap between recording intervals. Each 2 minute burst was averaged, giving a precision of 0.13 cm s^{-1} in the horizontal, and then rotated to give streamwise (U), cross (V) and vertical (W) flow components, for the full horizontal extent of the ADCP beams. To isolate tidal trends in the data so common flow characteristics may be ascertained; to facilitate understanding of common metrics that bring about the occurrence of CS, tidally averaged data was obtained by taking the mean of the rotated flow components over 17 tidal cycles between the dates of 03/07/2018 to 12/07/2018 in 30 minute divisions w.r.t. high tide.

The high precision sampling was continuous at 8Hz in 'Burst mode' giving measurements from 0.75 to 12.75 mab (depending on tidal height) with a 0.3 m resolution. These measurements used were collected over two tidal cycles from the morning of the 09/07/2019 to the 10/07/2019. This high precision data was used for both isolated vertical beam analysis and for obtaining contemporaneous flow components over the full horizontal extent of the ADCP beams. In the latter, 2 s beam data was first converted to Earth coordinate data and then rotated to give streamwise (U) and cross (V) flow components from 5 minute means. The component of vertical flow (W) was taken directly from the 5th beam. The Janus beams of the ADCP diverge with range, with a beam angle of 25° and cells of 0.3 m depth, this equates to a beam separation (diameter) gain of 0.28 m per cell, for example this gives 4.43 m separation at 5.25 mab.

The surface identification instrument package used in this work consists of a PointGrey BlackFly GigE Vision colour camera with a fixed 12 mm focal length installed in waterproof housing. With a resolution of 2448 x 2048 pixels, the camera provides 5 Megapixel images at a frame rate of up to 22 fps.

Images were captured with two frame rates; 1 shot every 15 seconds and 1 shot every 5 seconds allowing visual capture of 2.5 tidal cycles and 1 tidal cycle respectively, within storage capacity limits. The software FFMPEG [53] was implemented to convert these individual images into video with a time stamp overlay, allowing visual quantification of boil appearance on the sea surface within tidal cycles, as illustrated in the screenshot image capture in Figure 4, taken ∼1 hr 35 minutes before high tide on the 24th May 2018. A short excerpt of this video can be seen at `https://polychromatics.github.io/CoherentStructuresPaper`, which allows the reader to see the boils appear at the surface and then subsequently dissipate.

Figure 4: Screenshot of video capture with timestamp overlay top left of the image, illustrating boils seen at the surface above the ADCP position (green star) 1 hr 35 minutes before high tide on 24th May 2018. Accompanying video excerpt is available here: `https://polychromatics.github.io/CoherentStructuresPaper/`

Due to the non-linear nature of camera observations occurring due to storage and download times, uneven weighting occurred in some tidal periods. To alleviate this, half hour windows were defined with respect to high tide, then boil occurrences were normalised using the percentage of observation time in each of these windows.

2.2. Analysis Methods

In order to understand the magnitude and scales of temporal and spatial turbulence structures, analysis methods were applied using the 2 s ensemble averaged data from the vertical beam. Power Spectra Densities (PSD) were obtained from Fast Fourier Transforms (FFT) using Welch's segment-averaging method with 750-point (25-min) Hamming-tapered windows with 50% overlap.

Extending these FFT into time and frequency domains, the use of a wavelet element model (WEM) [54] gives time/scale information which represents real-valued time signals $x(t)$ composed of manifestations of the complex-valued element function $\psi(t)$ together with noise, and is given by:

$$x(t) = \sum_{n=1}^{N} \Re\left\{c_n \psi\left(\frac{t - t_n}{\rho_n}\right)\right\} + x_e(t) \tag{1}$$

where $\Re\{\cdot\}$ is the real part, N is the total number of events, c_n is the complex-valued amplitude and phase (when $i \equiv \sqrt{-1}$) of the nth event, giving t_n as its temporal location and p_n as the event scale, with $x_e(t)$ as the noise; which is assumed to be Gaussian and stationary and captures all variability not captured by the summation.

It should be noted that the output of the wavelet spectrum is not directly comparable to that of a Fourier spectrum in that the normalisation of the time-domain wavelets is amplitude, 1/s, as opposed to the more common energy, $1/\sqrt{s}$, which means that the output of the time-localised signals are more generally described by amplitude rather than an energy. This normalisation is employed in the optimisation process of fitting re-scaled and shifted versions of the wavelet functions because energy-normalised wavelet transforms are overly influenced by variability at adjacent times. This means that analysis of time series containing multiple, potentially interactive, events can mean that maxima are achieved when all events are spanned, rather than having the ability to detect individual events. Thus the power captured by a wavelet at a particular time/scale point in the wavelet element model (WEM) is the same as a wavelet transform with an amplitude normalisation and is therefore the model based on the principle of optimising power [54].

For subsequent turbulence analysis application of Reynolds decomposition was undertaken, separating the beam velocities, b, into mean, $\overline{b}$, and perturbation, b', using 5-minute means; determined to be the longest duration with stationary statistics and the shortest to capture the variance in the signal, which satisfies the assumption of homogeneity and stationarity.

$$b = \overline{b} + b' \tag{2}$$

The Turbulence Intensity (TI) is the ratio of the turbulence fluctuations (standard deviation of the velocity (σ), i.e. the square root of the variance) to the mean flow, with a noise-corrected term subtracted for acoustic Doppler measurements [6, 55]. TI can be calculated in all three dimensions (I_u, I_v, I_w). Along stream one dimensional TI used in this study is defined as:

$$I_u = \frac{\sigma_u}{\overline{u}} = \frac{\sqrt{\overline{u'^2} - n^2}}{\overline{u}} \tag{3}$$

The TKE dissipation rate ϵ is calculated using the second-order spatial structure function from the raw along-beam velocities [56, 40, 57] defined as:

$$D(z,r) = \overline{[b'(z) - b'(z+r)]^2} \tag{4}$$

where z is the along beam position and r is the separation distance.

Assuming isotropic turbulence in the inertial subrange, D is related to dissipation ϵ by

$$D(z,r) = C_v^2 \epsilon^{2/3} r^{2/3} \tag{5}$$

where C_v^2 is a constant taken to be 2.1 and $D(z,r)$ has the form $Ar^{2/3} + 2\sigma_v^2$ with σ being the variance of velocity estimates at a point due to the instrumental noise.

The along and cross stream Reynolds stress estimates from the along beam variances were obtained [58, 59];

$$-\frac{\tau_x}{\rho} = \overline{u'w'} = \frac{\overline{b_2'^2 - b_4'^2}}{2\sin 2\theta} \tag{6}$$

$$-\frac{\tau_y}{\rho} = \overline{v'w'} = \frac{\overline{b_1'^2 - b_3'^2}}{2\sin 2\theta} \tag{7}$$

where ρ is the density, $b_n'^2$ are the various along and across flow beam velocity variances, as shown in Figure 3, and θ is the angle each beam makes with the vertical; 25° for this instrument.

It should be noted here that Lohrmann et al. [58] find that an additional correlation term $\overline{u'v'}$ in the Reynolds stress estimates can be neglected provided the tilt angles of the instrument are $< \pm 8°$. Moreover, if horizontal and vertical variances are of the same order then contribution from terms that involve the differences of these variances may also be neglected, but that this assumption does not hold in the presence of surface gravity or internal waves.

Multiplying the Reynolds stress by the velocity shear provides an estimate of the rate at which energy is transferred from the mean flow to turbulent kinetic energy; the rate of production of turbulent kinetic energy (P) [48], according to:

$$P = -\tau_x \frac{\partial \overline{u}}{\partial z} + \tau_y \frac{\partial \overline{v}}{\partial z} = -\rho \left(\overline{u'w'} \frac{\partial \overline{u}}{\partial z} + \overline{v'w'} \frac{\partial \overline{v}}{\partial z} \right) \tag{8}$$

Obtaining Reynolds stresses and P relies on the condition of temporal stationarity [59], implying that the timescale for the evolution of the flow must be much longer than the timescale for the calculation of the Reynolds stress, or that the covariance between beams is much less than the variance of the individual beams. This allows elimination of the covariance terms. A second condition is that of spatial homogeneity, requiring that opposite beams are sampling the same turbulence statistics. Lastly, vertical bin size implies that eddies of a size smaller than 60 cm (or two bins) will not be resolved, resulting in an underestimation of the variance in the velocity field. In general situations, this contribution will be small, as the Reynolds stresses and P are dominated by the larger scales.

2.3. Assumptions and Noise

In the following analyses utilisation of Taylors "frozen field" assumption [60] is applied for horizontal advection with the mean speed $\overline{u}$ giving a length-scale L for frequencies f such that:

$$L = \frac{\overline{u}}{f} \tag{9}$$

acknowledging that if the turbulence evolves faster than it is advected, length-scales could be aliased. For single beam measurements this implies that the coherent structures must be travelling close to the mean flow speed, and for methods utilising velocities from opposing beams it has the implication that distances smaller than the ADCP beam spread can not be evaluated [7].

The uncertainty in the estimates (arising from the Doppler noise) is different for each analysis method. The turbulent kinetic energy production (P) utilises means and variances ensemble averaged over 5 minutes, leading to noise levels of 0.002 m s^{-1} (taking the horizontal noise level of 0.09 m s^{-1} and dividing by $\sqrt{}$(number of pings) [61]). All data analysed using the vertical beam was ensemble averaged to 2 s to improve SNR; with vertical beam noise quoted as 0.058 m s^{-1} this gives noise levels of 0.014 m s^{-1}. The vertical beam was tilted to an angle of 5.4° which results in a bias in the vertical beam estimate of ∼1% of the horizontal velocity, which does not significantly affect the vertical velocity estimates in this study.

3. Observations and Analysis

Over the study period a total of 55 hours of video observations were performed. 42 hours with a repetition rate of 1 shot every 5 seconds between the 2$^{\text{nd}}$ May and the 11$^{\text{th}}$ July 2018, with 19, 9 and 14 hours of observations in each month respectively. In addition, a 13 hour full tidal cycle examination was completed on 8$^{\text{th}}$ July 2019 with a repetition rate of 1 shot every 15 seconds. It is assumed that free–surface boil activity represents water column coherent structure activity; knowing when coherent structures impinge on the free surface allows scrutiny of the marine environment to validate techniques for coherent structure observation.

Boils were observed above the ADCP for a total of 19 of the total 55 hours, i.e. 1/3 of the tidal cycle is 'boily' in this location. Figure 5 compiles the normalised observations of boil occurrence w.r.t high tide over a tidal cycle, suggesting the likelihood of CS activity. These observations are delineated into half hourly divisions, hereafter named 'tidal slices'. Overlain is sea surface height and depth-mean flow direction, together with tidally averaged velocity components. The figure shows that the flow is not symmetric. Flow from low tide until 1.5 hours before high tide the mean flow direction lies along a compass bearing of 235°, the flow then rotates to a mean of 207° from North until 2.5 hours after high. Over the next ∼3.5 hours the flow direction reverses and then settles back at 235° from North at low tide and the cycle starts again. Streamwise depth mean flow velocity above the ADCP is less than that of the main channel, with flow above the ADCP peaking at a tidal average of 0.8 m s^{-1} approximately 1 hour 30 minutes before high tide. Higher velocities are observed during the flood tide and reduce rapidly on the ebb, dropping to 0.04 m s^{-1}.

The peak in boil occurrence lies within the 30 minute period immediately before high tide, with the distribution of boil occurrence weighted towards the flooding tide. No boils are observed in the time window of 2 hrs 30 min after high to 5 hrs 30 min before high. Within this window the flow above the ADCP changes direction and the streamwise velocity drops to its minimum value of 0.04 m s^{-1}. Within the period of boil occurrence a minima occurs in the half hour time period starting at 2 hr 30 min before high tide which coincides directly with the change in main channel flow direction, obtained visually from 5 different dates to be 2 hrs 21 min before high. This is not coincident with the flow direction change over the ADCP, which commences at ∼3 hrs after high tide.

The tidal trends in Figure 5 shows that boil occurrence was observed to coincide with maximal tidally meaned cross and vertical flow components

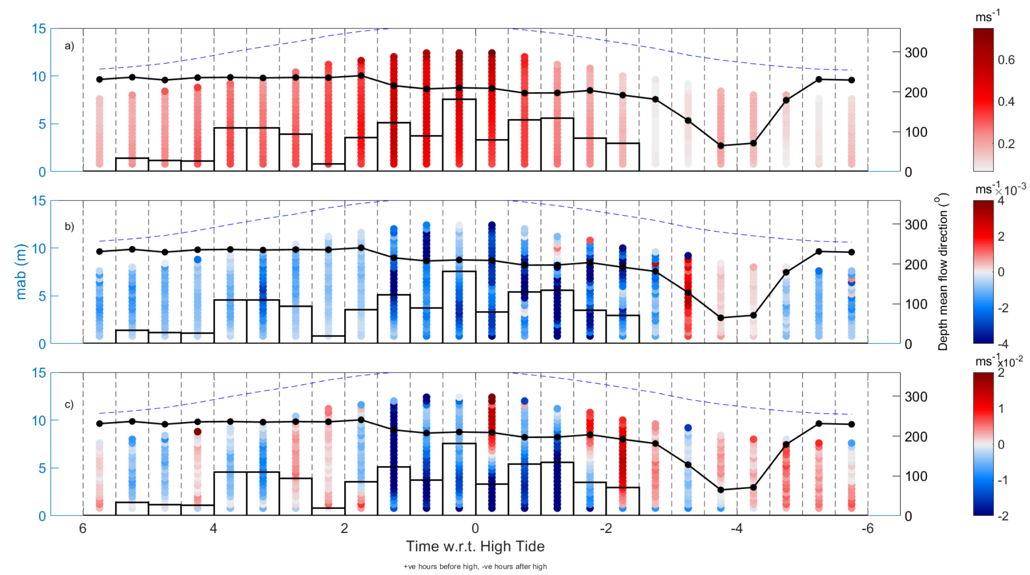

Figure 5: Histogram showing normalised boil occurrence (black, arbitrary scale) with depth–mean flow direction (black), sea surface height (blue dashed line) and tidally averaged streamwise flow velocity components (colour–scale) with; a) U, streamwise flow b) V, across stream flow c) W, vertical flow. Time given in hours from high tide point, with +ve being hours before high and -ve being hours after high.

with a lesser correlation to streamwise flow magnitude. Correlations were computed for boil occurrence to absolute tidally averaged flow components, giving R^2 values of 0.21, 0.32 and 0.43 for streamwise, cross and vertical respectively. Scrutiny of Figure 5 reveals a proclivity for boils when the vertical flow component is downward, thus this constituent was isolated and correlated with boil occurrence, giving an R^2 value of 0.73.

Figure 6 shows the individual rotated components over the period of interest (July 09-10 2019) from the ADCP 'Burst mode' velocities. It is evident that trends are apparent but there are tidal variations day to day.

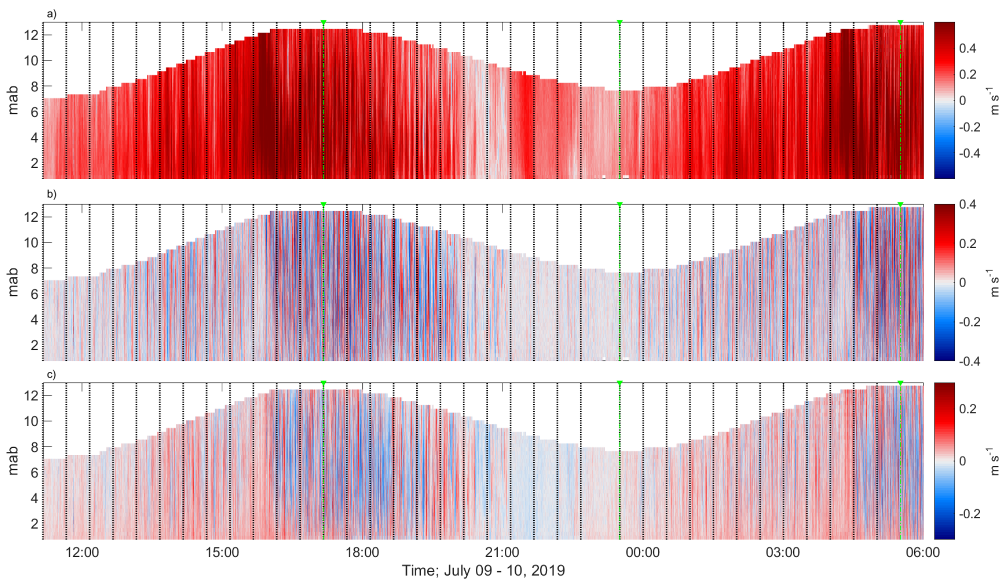

Figure 6: High precision ADCP flow components a) streamwise and b) cross flow. c) vertical velocity estimation from beam 5. (note the different scales). Black dotted vertical lines denote tidal slices and green dotted vertical line with green arrow above denotes high and low tide positions

Generally, there is as a peak streamwise flow magnitude in the tidal slice 1.5 hours before high tide, immediately subsequent to the flow direction change from 235° to 207°. The streamwise flow magnitude drops above the ADCP when the main channel flow changes direction. Maximal cross flow components are evident in the period when the flow is directed to 207°; often peaking when the streamwise flow component drops, the same is evident in the vertical component. Flow is not uniform across depth, with strongly sheared boundary layers ostensible in the streamwise flow component both from the bottom boundary and to an extent within the resolvable surface boundary. These effects are particularly evident during higher streamwise velocities as this bottom boundary layer extends further up the water column in this regime.

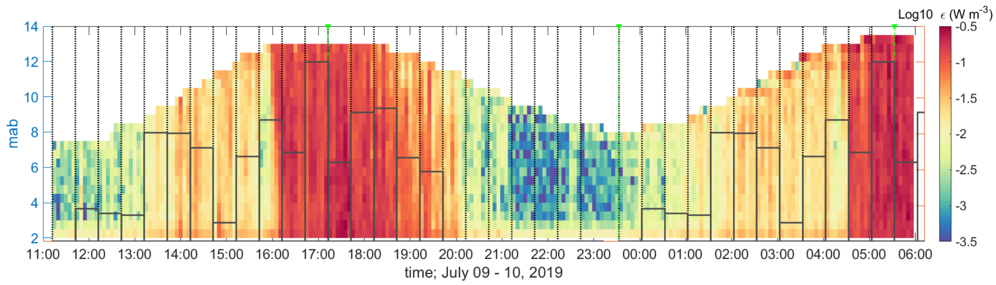

Figure 7: Turbulence Kinetic Energy Dissipation from the Structure Function geometrically meaned across all beams. Vertical black dashed lines denoting the tidal slices and the vertical green dashed lines with triangle over denoting the high and low tide positions. Boil occurrence histogram overlain in grey.

Figure 7 shows the turbulence dissipation rate estimates from the temporal Structure Function technique, Eqn 4 and 5, obtained for each beam with the bottom bin masked due to transducer proximity artefacts. Data was then depth mapped and geometrically meaned across all beams, with the boil occurrence histogram overlain. Figure 7 illustrates elevated dissipation across the whole of the bottom boundary, regardless of tidal period, with maximal estimated dissipation in the tidal slices 1 hour before high tide to 2.5 hours after high tide, which is also when the streamwise velocities have shifted in direction from 235° to 207° from North (Figure 5). The periods of maximal dissipation coincide with peaks in cross flow velocities (Figure 6). TKE dissipation magnitude does not correlate with boil occurrence, although dissipation is elevated when boils are present and there is a variance in elevated dissipation mid-water during the periods of free-surface boil activity which could be due to coherent structure prevalence; energy in these structures could be advected downstream.

Metrics are required that allow coherent structure characterisation, by way of spatial and temporal structure, within the water column using an ADCP. The vertical beam of the Nortek Signature 1000 facilitates the direct analysis of vertical flow components, without the need for modifications to the flow components required with Janus configuration sonar beams.

Fast Fourier Transforms (FFT) with utilisation of Welch's method were employed to the 30-minute tidal slices across the whole observation period to ascertain if there are high frequency repetitions of a sinusoidal nature in the vertical beam velocities that could be attributed to coherent structures.

On analysis there were no repeating patterns over 10 minutes that contained any significant energy in the Power Spectral Density (PSD), the majority of the energy being found in the sub 6 minute region. Restricting our observations to the period of quoted coherent structure lengthscales in the literature, which is 21.5 ± 22.3 m for the studies quoted in the introduction, leads to repetition times of 57 seconds. Figures 8 and 9 are limited to maximum extents of 2 minutes, which is the mean plus one standard deviation of the literature coherent structure lengthscales. These figures show the FFT plotted across all depths in 30 minute tidal slices, one for the pre-high and one for the post-high tide on the 09/07/2019.

Figure 8 shows energy in the water column for the first 3 hours (6 x 30-minute tidal slices) after high tide. These peaks in energy are generally found

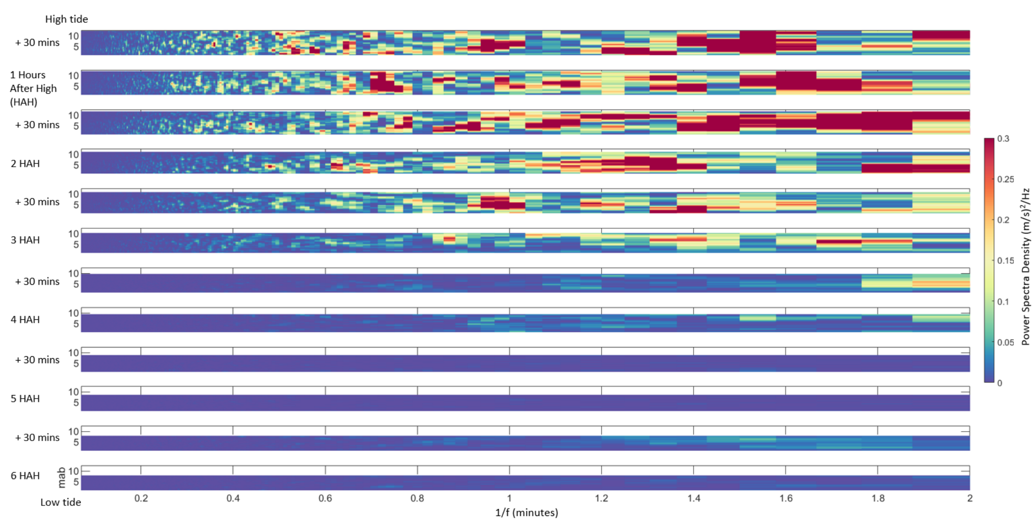

Figure 8: Post-high tide FFT stacked in 30 min time slices from high to low tide top down

at specific depths in the 30-minute FFT window. Longer period elevated PSD is ostensible across larger depth ranges.

In the pre-high tide 30-minute tidal slices shown in Figure 9 the elevated PSD does not occur until 2 hours after low tide, the 5th panel from the top in the figure. Subsequent to this there is elevated PSD in all tidal slices with the exception of the slice 1.5 hours before high, 3rd panel up from the bottom; when the streamwise velocities are at maximum.

These findings correlate extremely well with free-surface boil occurrences; i.e. there are low period signals apparent in the FFT when boils are present suggesting these are associated with coherent structures in the water column. The peaks in PSD range from minima of 0.11 minute to the 2 minute periods scaled here, leading to coherent structure lengthscales of ~ 2.5 to 46 m when converted assuming Taylors "frozen field" with a mean flow of 0.38 m s^{-1}.

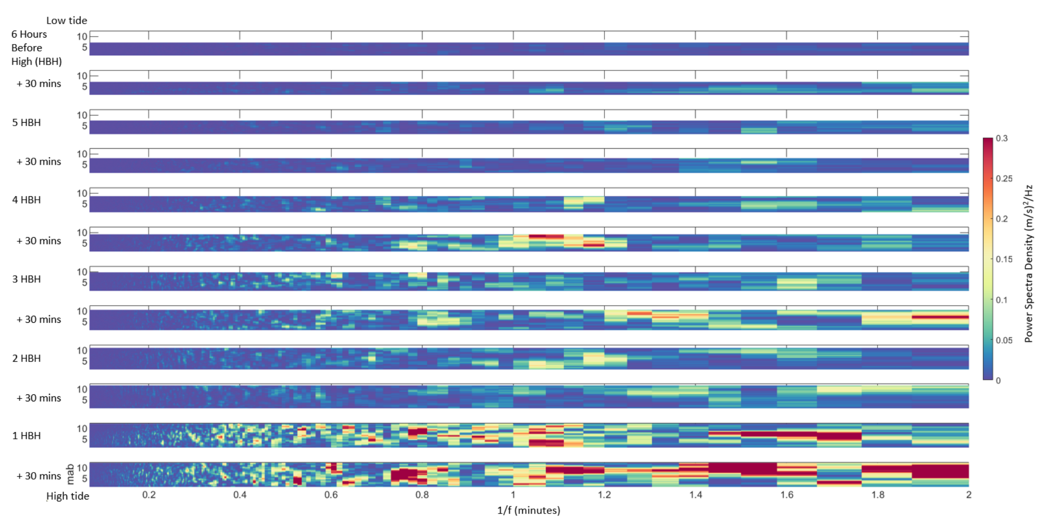

Figure 9: Pre-high tide FFT stacked in 30 min time slices from low to high tide top down

The FFT illustrates peaks in PSD over a full 30-minute window, so any depth tendency is integrated over this time period. In order to extrapolate this information further one requires time-localised periods, which can be carried out using wavelets.

Figure 10 utilises the wavelet element model (WEM) of Lilly [54], by first detecting the wavelet transform maxima using a generalised Morse wavelet of γ 2 and β 2, $\psi_{2,2}(t)$, then by examination of the time/scale distribution of these transform maxima due to assumed Gaussian white noise; a level of statistical significance using Monte Carlo methods is determined. Lastly, by applying a criterion to verify that each event is sufficiently isolated from one another based on an expected region of influence (ROI) associated with a transform maxima, one can visualise significant features which are a good match to the element function [62].

Figure 10 illustrates the application of the WEM to the depth bin at 5.25 mab for the full ∼1.5 tidal cycles in this study, (July 09-10 2019). It is clear that the WEM emulates a good approximation for surface boil activity and thus coherent structures in all instances except when the streamwise velocities are maximum, in the tidal slice 1.5 hours before high; where the vertical velocities are minimal.

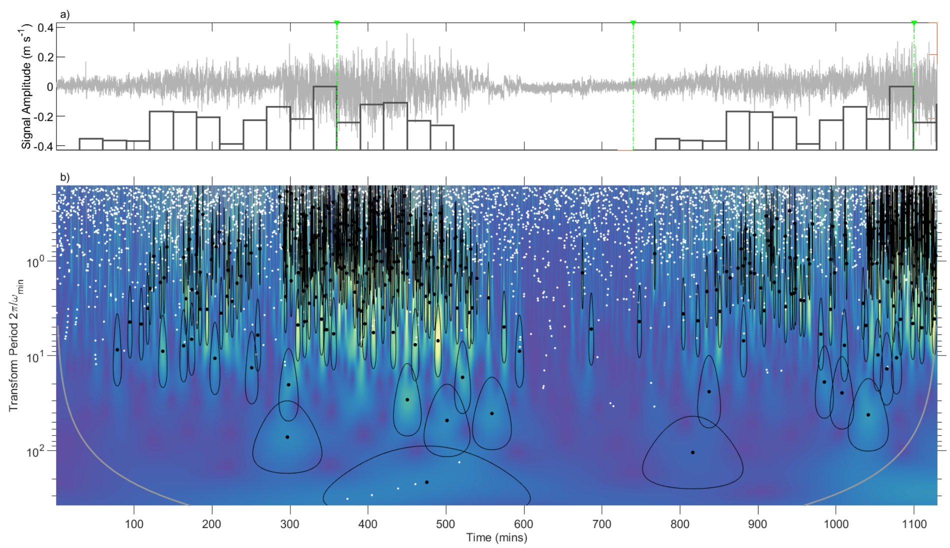

Figure 10: a) vertical velocities at 5.25 mab for the full ∼1.5 tidal cycles in this study; which gives the input signal amplitude in m s^{-1}, with vertical green dashed lines with triangle over denoting the high and low tide positions and boil occurrence histogram overlain in grey. b) WEM of the same period, using wavelet $\psi_{2,2}(t)$ with transform period $2\pi/\omega_{min}$ on a logarithmic y-axis, black dots marking the locations of the statistically significant and isolated maxima while white dots marking the locations of other transform maxima. The black circles delineate the $\lambda = 1/2$ region of influence (ROI) around each maxima. The cone of influence is shown.

To study the WEM outputs in more detail, Figure 11 takes the wavelet spectrum of the 30-minute tidal slice directly after high tide on 09/07/19 at 5.25 mab, with transform maxima, statistical significance and ROI illustrated. This smaller section of data allows lengthscales to be determined by scaling with the mean flow. There are 15 significant events in this window, 13 of them being $\leq$ 2 minutes period, with the most powerful at 26.4 minutes into the time window having a transform period of 0.26 $2\pi/\omega_{min}$. Again assuming Taylor's "frozen field", with the mean streamwise velocity in this tidal slice of 0.44 m s^{-1}, this gives a coherence lengthscale of 6.8 m. The average lengthscale for all these 15 features is 34.5 $\pm$ 41.7 m, with a median of 19.5 m and the 5 highest amplitude features are 16.9 $\pm$ 11.2 m with a median of 13.2 m.

Figure 12 shows the same 30-minute tidal slice directly after high tide, stacked by depth above bed and limited to wavelet spectra of 0.1 to 2 minute transform periods. The minimum value of significant transform maxima over all these depths is 0.17 $2\pi/\omega_{min}$ leading to a lengthscale of 4.49 m. Trends of high amplitude pathways extend up from the seabed, repeating with an average periodicity of $\sim$127 s. Taking the transform periods of these pathways alone, 7 in this tidal slice, and scaling by mean streamwise velocity, an average boil lengthscale of 22.2 $\pm$ 11.9 m is obtained. These features increase in transform period by height above bed, initially exhibiting average lengthscales of 14.9 m extending to 29.5 m. Observing a general trend, many features progressing upwards in the water column also increase in time on the x-axis, suggesting advection and vertical movement. Calculating the time translation for the 7 pathways identified to exhibit this trend indicates

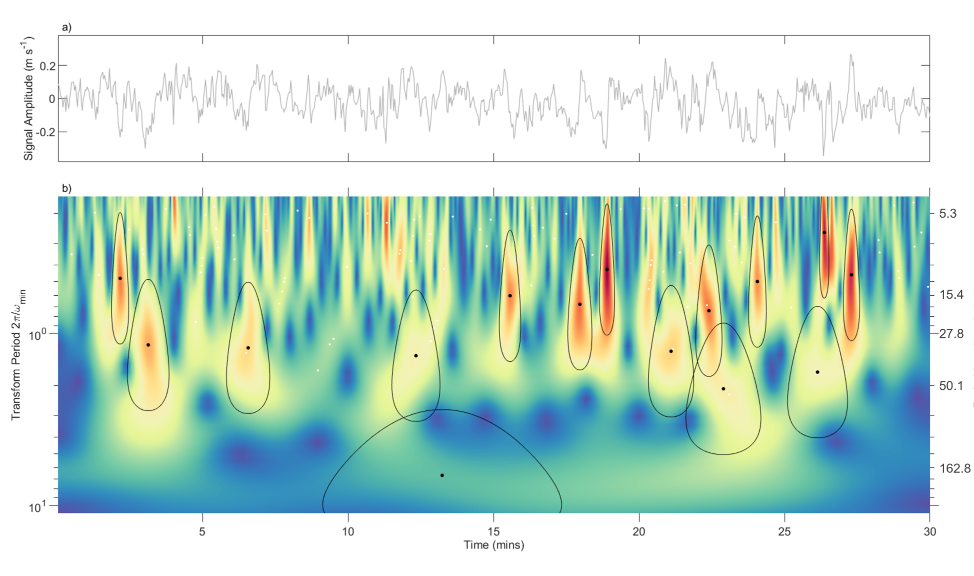

Figure 11: a) vertical velocities at 5.25 mab for tidal slice directly after high on 09/07/2019 starting at 17:10, giving input signal amplitude m s^{-1}, b) WEM of the same 30 minute tidal slice input signal, using wavelet $\psi_{2,2}(t)$ with transform period $2\pi/\omega_{min}$ on a logarithmic y-axis, black dots marking the locations of the statistically significant and isolated maxima while white dots marking the locations of other transform maxima. The black circles delineate the $\lambda = 1/2$ region of influence (ROI) around each maxima. The right hand axis shows the approximate lengthscale, scaled by the mean speed for the tidal slice of 0.44 m s^{-1}

coherent structures moving with an average speed of 0.48 m s^{-1}, which is 109 % of the mean streawmwise velocity. Withal suggestive of vertical movement and expansion; further analysis of these features is warranted to observe progression in the water column over many tidal slices to obtain reliable statistical means. However, this is outside the scope of this present paper.

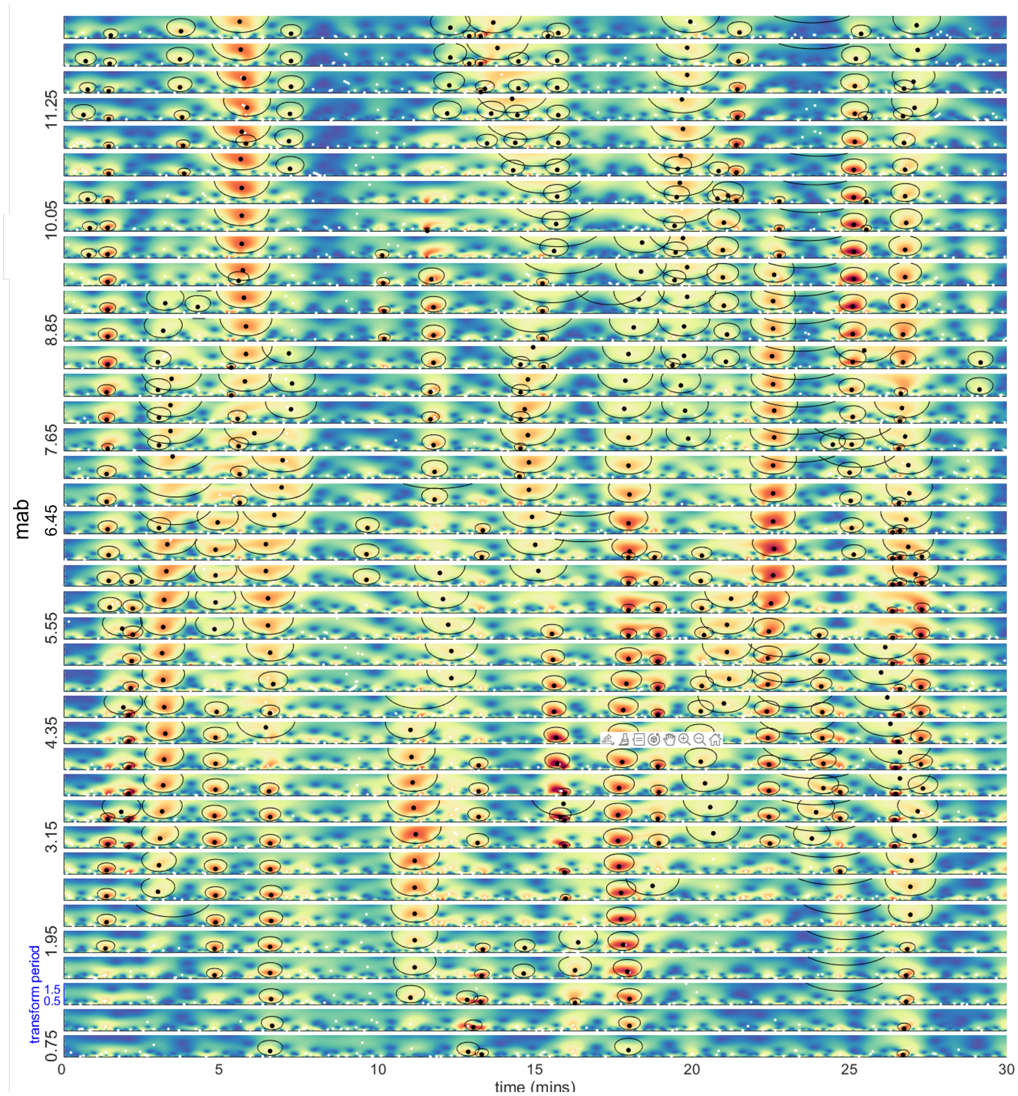

Figure 12: WEM of the 30 minute tidal slice directly after high tide on the 9th July 2019 starting at 17:10. Each stack shows the transform periods (blue axis label) from 0.01 to 2 $2\pi/\omega_{min}$ stacked by depth bin, with mab shown every 4 stacks (black axis label). The wavelet used is $\psi_{2,2}(t)$ with transform period $2\pi/\omega_{min}$ on a logarithmic y-axis, black dots marking the locations of the statistically significant and isolated maxima while white dots marking the locations of other transform maxima. The black circles delineate the $\lambda = 1/2$ region of influence (ROI) around each maxima.

Figure 13 shows Turbulence Intensity and TKE P, obtained via the variance method, Eqn. 8 with contributing Reynolds stresses and Shear shown below. Here a mask has been applied when the mean streamwise velocities are outside $10°$ of alignment with beams 2 and 4, which masks the most energetic regions, but leaves a period of active free-surface boil observations for coherent structure prevalence cross-analysis. It is apparent that the turbulence intensity is not at all indicative of coherent structures, as seen with the overlain boil occurrences. Moreover, on comparison with Figure 7 it appears that it is also an insufficient method to illustrate the TKE dissipation in the water column.

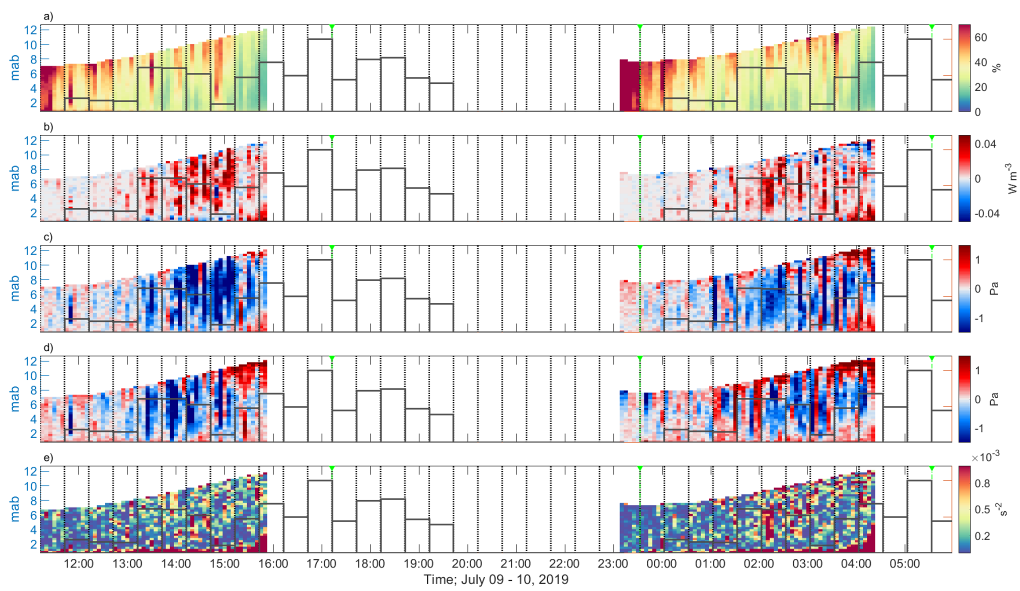

Figure 13: a) Turbulence Intensity b) Turbulent Kinetic Energy Production from the variance method c) $\overline{u'w'}$ Reynolds stress d) $\overline{v'w'}$ Reynolds stress e) Shear squared. Vertical black dashed lines denoting the tidal slices and the vertical green dashed lines with triangle over denoting the high and low tide positions. Boil occurrence histogram overlain in grey.

In Figure 13 it is apparent that the periods of elevated P are mainly above the boundary layer and elevated when there are coherent structures in the water column. Negative P is apparent occasionally near the surface boundary and mid depth in the water column, with bottom boundary occurrences in mid tide; this phenomena is explored in the discussion. Over the two tidal cycles in this study, it can be seen in Figure 13 that there are peaks in shear in the bottom boundary, but also mid-water when associated with periods of free-surface boils and thus assumed water column coherent structures. Accompanying these peaks in shear are periods of elevated P, with some periods when the P term is negative.

Generally, when the momentum flux, $\overline{u'w'}$, is maximum and the $\overline{v'w'}$ stresses are small or negative, negative P is observed. These stresses suggest that ejection events dominate momentum transfer[63], which is indicative of coherent structures present in the water column [18]. Furthermore, Figure 14 indicates that depth meaned TKE production and dissipation are not conserved in the water column suggesting a redistribution of momentum.

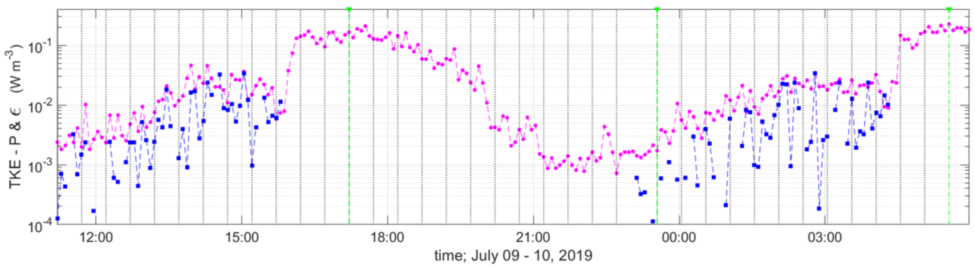

Figure 14: Turbulent Kinetic Energy Production from the variance method, depth meaned (blue squares), Turbulence Kinetic Energy Dissipation from the Structure Function geometrically meaned across all beams then depth meaned (magenta circles). Vertical black dashed lines denoting the tidal slices and the vertical green dashed lines with triangle over denoting the high and low tide positions.

The WEM was run over all depths for the 9^{th} tidal slice after the second low tide (not shown), starting on the 10/07/20 at 03:30; this slice being chosen as it is a period of significant free-surface boil activity and thus assumed coherent structure activity and also a period with many instances of negative P. 24 instances of statistically significant wavelet transform maxima were found to correlate with peaks in negative P within a 2.5 minute time window and for the same depth bin.

Converting transform maxima periods of less than 3 minutes, (which captures 21 instances, all but 3 of the total falling within corresponding depth bins), to lengthscales using the mean streamwise velocity for this tidal slice, being 0.29 m s^{-1}, they range from 3.8 to 51 m with a median of 9.9 m. Beam separations at these depths range from 0.5 to 9.8 m with a median of 8.1 m. Of these instances, 8 fall within a 2 m difference from lengthscale to beam separation; 3 less than 2 m, 2 less than 1 m and the final 3 less than 0.5 m difference. The minimum significant transform maxima over all depths for this tidal slice is 0.19 $2\pi/\omega_{min}$ leading to a lengthscale of 3.3 m.

4. Discussion

This work has undertaken to identify measurable metrics for characterisation of marine turbulent macroscale coherent structures and their spatial and temporal configuration in tidally energetic channels, for utilisation by the tidal energy sector. Firstly, this discussion will concentrate on the surface boil identification and follow this with the ADCP analyses discussion; focusing on the vertical beam metrics, starting with larger tidal period and following with the tidal slice focused study. The section finishes with discussion on variance method metrics.

It is assumed that periods of free-surface boils are accompanied by coherent structures within the water column and thus observations of free-surface boil occurrence were first carried out so that ADCP analysis methods could be aligned accordingly. The boil observations were carried out 'by eye' and boils were noted when there was a smooth 'boil signature' on the water surface, as illustrated in the screenshot in Figure 4 taken from `https://polychromatics.github.io/CoherentStructuresPaper`. This however, is arbitrary, and does not necessarily mean that there is a period of active coherent structures/'boiling' within the water column at the study site at that time. The smooth patch/boil signature could simply have been advected over the ADCP in these periods; no information has been obtained in order to differentiate these phenomena. That being said, the correlations with the metrics here seem sound. Future work could be undertaken to parametrise a systematic free-surface boil detection, which could incorporate 'flow into' the capture space to reduce these uncertainties.

The prevalence of boils is high for ± 2 hours around high water and evident on the flood tide from up to 4 hours before high, with the highest occurrence being in the 30 minute period before high tide. Boils are observed only on the flooding tide, when the streamwise flow direction above the ADCP is from NE to SW. Boil occurrence being absent on the ebbing tide, when the flow is is from SW to NE, could be due to a lack of boil initiation points in the channel upstream of the ADCP; as boils are observed at different locations in the channel, but it could also be related to boundary layer structure differences in the water column during flood and ebb as seen by Hay et al. [38]. Further work with close observation of the boundary layer structure with an ADCP would be able to tease out the likelihood of one of these suppositions.

There is an obvious lack of boil occurrence above the ADCP when the main channel flow changes direction in the 30 minute period of 2 hr30 to 2 hours before high tide, seen in the boil histograms, which suggests localised flow direction changes can affect boil occurrence. These two locations (main channel and ADCP location) are separated by $\sim 110 - 180$ m (edge and centre respectively) and have a depth difference of $\sim$7.3m at the central extent. Boils were also evident in the main channel from the image observations, and thus these findings suggest significant site specific spatial variability in the occurrence of coherent structures which should be taken into account when turbine location is selected.

For this section of the analysis we use 1.5 tidal cycles sampled at high resolution, (6, with focused study around the first tidal high. The vertical beam of the ADCP facilitated the direct analysis of vertical flow components, and metrics utilising this beam were analysed along with variance method metrics obtained from averaging over the Janus configuration sonar beams.

Fast Fourier transforms (FFT) illustrated peaks in power spectral density (PSD) concurrent with coherent structure activity, with low period/high frequency signals apparent in the FFT correlating with periods from 0.11 minutes up to 2 minutes implying lengthscales of 2.5 to 46 m. Spectral peaks appeared at different depths in the water column, suggesting contained structures, but as the FFT is integrated over the 30-minute tidal slice there is no way of knowing 'when' these structures appear, i.e. there is no time-localised identification. Wavelets are a method of extracting time-localised periodic information from velocity time series that can be described by signals that are non-sinusoidal in nature. Keylock [64] provides a technical communication as to how this can be utilised to visualise turbulent coherent structures. If one wishes to optimise tidal energy power extraction so that it does not fall foul of coherent structure damage time localised information could prove useful, in fact this technique has already been used by the wind energy sector. Kelley et al. [8] uses these techniques to observe large loading events on wind turbine rotor blades associated with coherent structures, Thomson et al. [61] use the same technique to observe coherent turbulence from an ADV in a tidally energetic channel, finding energy in low and high frequencies but with high frequency structures being difficult to observe, and Salim et al. [43] utilise wavelet power spectra to examine the role of coherent structures in incipient sediment motion by way of momentum and sediment flux. Lilly [54] establishes significance and region of influence element analysis in the time/scale plane with application of an element model directly inspired by continuous wavelet analysis to oceanic eddies.

Figure 10 illustrates a full tidal cycle WEM output, representing an overview of the ability of the WEM to define the CS likelihood, with the possibility to emulate this for all depth bins or the depth bin of interest for the application at the time. The WEM gave good correlation to boil observations in all but the tidal slice 1.5 hours before high, when the streamwise velocities were maximal and the vertical velocities were minimal. This window could be significant for the tidal energy sector; as there is a minimum flow magnitude (cut in speed) in order to provide power output [65, 66, 67, 68, 69, 70]. The two metrics could be anti-correlated as the tidal slices chosen were referenced to high tide and did not exactly match up with this higher streamwise speed event; there was some overlap into a period of increased vertical velocity magnitude. On scrutiny of the video captures, boil observations were noted to be particularly prevalent at the end of this time window/tidal slice, which would support this supposition. This could lead to surface boil/coherent structure activity that appears to be in this tidal slice but is not observed in the WEM. Further scrutiny of such events in future studies at tidal energy sites would be wise to understand coherent structure activity correlation with the maximal power range of tidal turbines.

This WEM was then utilised to examine the highly energetic 30-minute tidal slice of the tidal cycle directly after high tide, a period of known high surface boil activity (Figure 5). Studies looking at coherent structures within lab, river and sea environments [17, 16, 11, 10, 20, 21, 22, 14, 6, 7, 18, 12, 13, 24, 23] place coherent structure length scales anywhere in the region of

1 – 80 m. Furthermore, isolating these studies to environments at sea gives lengthscales of 21.5 ± 22.3 m [15, 19, 13, 6], where scaling by the water depth and taking an average one obtains a ratio of 0.6 h.

The WEM for the tidal slice found that the largest amplitude peak in wavelet transform period lay at a lengthscale of 6.8 m, with the 5 most powerful features in this period giving lengthscales of 16.9 ± 11.2 m with a median of 13.2 m. Scaling this by water depth for this tidal slice gives 0.9 h for the median lengthscale and 0.4 h for the largest amplitude. The lengthscales of interest to the tidal energy industry correspond to tidal turbine rotor diameters and blade cord lengths commonly quoted to be $\mathcal{O}10$ m and $\mathcal{O}1$ m respectively, and as such this study suggests that these features lie well within this tolerance, implying the wavelet technique is efficacious.

Figure 12 shows depth stacked model outputs for the transform periods of 0.01 to 2 $2\pi/\omega_{min}$ over all depth bins. We would expect a periodicity of CS ejection events to be related to an intrinsic timescale of the flow. Heathershaw [12] carried out a study in the Irish Sea in depths of 10 – 60 m with currents of the order of 1 m s^{-1} and found ejection and sweep events falling between 5 to 10 s, corresponding with maxima in the Reynolds stress cospectrum, with a periodicity of 20 to 100 s. Isolating significant peaks in figure 12 that extend from the seabed towards the water surface, a periodicity of 127 s is obtained; a similar finding for a similar flow regime. Moreover, many of the significant peaks in the figure are seen to advance in the x-axis time window with movement upwards in the water column, with such events moving at $\sim$ 0.48 m s^{-1} which is 109% of the mean streamwise velocity. Adrian and Marusic [28], Nimmo Smith et al. [15], Steele et al. [71] find speeds ranging from 80 – 117% of the mean streamwise velocity. The findings suggest that these features are likely to be redistributing momentum throughout the water column. In order to ascertain the robustness of these findings a statistical approach should be used on many such tidal slices over many tidal cycles; an exercise which is beyond the scope of this work. Nevertheless these findings are promising.

A large body of literature exploring the influence of turbulence on tidal energy turbines utilises the metric of turbulence intensity (TI), obtained from the ratio of the square root of the variance across beams to the mean flow. Moreover the turbulent kinetic energy production (P) is evaluated from the product of the Reynolds stress, calculated across beams, and the velocity shear. As mentioned in section 2.2 to calculate variance terms an assumption of independence, drawn from temporal stationarity, means that instantaneous velocity measurements from one beam must be independent from another, i.e. the characteristic size of the eddies is significantly less than the beam spread, which allows elimination of the covariance terms leaving only the variances in the measured along beam velocities as a source for higher order calculations. If one draws the conclusion that there are coherent structures in the water column with sizes comparable to beam spread, as is common in tidal races, then this implies that variance based estimates could be prone to bias.

In this study it is apparent that the periods of elevated P are above the boundary layer and not decreasing with increasing height as is characteristic for wall-bounded turbulence [72, 4, 73, 74, 48] and negative P is apparent in the water column as is also observed by the same quoted literature.

Generally, regions of high P are associated with locations of maximal mean stress and shear which ordinarily occur near the boundary. Korotenko et al. [73] find stress profiles departing from this tendency at times when other mechanisms contribute to the Reynolds stresses in the upper layers and attribute this to a "curling back" of the stress profiles. They ascribe negative P estimates to unreliable stress estimates during the turning of the tide. Lu et al. [72] also observe negative P, attributing it to unreliable stress estimates occurring from sign reversal of stress and shear. Rippeth et al. [48] find anomalously high stress estimates in the upper part of the water column and also a "curling back" of stress which they attribute to instrument noise associated with contamination by wave orbital velocities and a lack of coherence between stress and shear leading to a failure of the 'significance of covariance test' and periods of negative P near to the surface.

Coherent structure occurrence as identified via the WEM often correlated with periods of negative P. Identifying the depth and time of these correlated events and scaling the transform periods gave coherent structure lengthscales comparable to that of the beam spread. Statistically significant transform maxima periods, scaled with mean velocity, gave lengthscales from 3.8 to 51 m, while beam spread ranged from 0.5 to 9.8 m. Eight instances of correlated coherent structure lengthscales and beam spread at the corresponding depth gave differences in these two lengthscales of less than 2 m, three of these being less than 0.5 m. Clearly these coherent structures are within the bounds of beam spread where we are seeing negative P. Moreover it is clear from Figure 11 that the significant peaks in transform energy (black dots) are within bounds of regions of influence of these maxima (black circles), thus transform periods captured and converted to lengthscales from the statistically significant maxima alone will not necessarily capture the full size range of the coherent structure, being ‘smeared’ across transform periods.

This brings into question the usage of variance across beams when coherent structures are present in the water column, as is often the case in tidal races where tidal energy turbines are to be placed. This could be due to a covariance between the beams from the coherent structures meaning the fundamental assumptions lain out by Lohrmann et al. [58] and Stacey et al. [59] in the cancelling of terms so that the Reynolds stresses can be obtained by variance alone, are no longer valid in these cases. This is illustrated in the schematic 15.

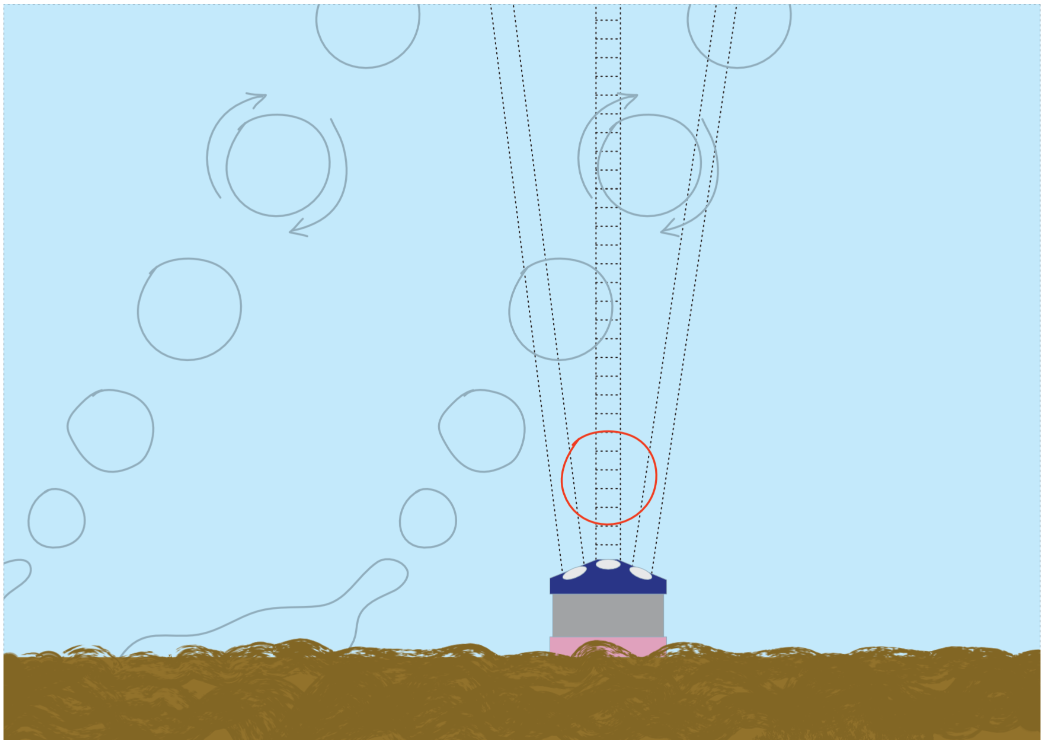

Figure 15: Schematic representing the ADCP Janus and vertical beam and coherent structures present in the water column.

Furthermore, obtaining energy balances from the relation between dissipation and P, when the the ADCP variance method has been used in locations where coherent structures are likely could prove problematic as the variance method could under-estimate P due to its limitation in combining beam estimates, which are not present in the Structure Function ϵ estimates; this is suggested in the magnitudes of both estimates found here as shown in Figure 14. Elevated dissipation, obtained from the Structure Function, is apparent throughout the water column when coherent structures are present, with considerable mid-water structure (Figure 7), this could be more deeply investigated with further study given time.

Negative P is observed in the bottom boundary in this dataset that does not fit with the findings above due to the beam spread being small; with a spread of only 20 – 50 cm in the bottom bins, negative P estimates would be expected to correlate with height and beam spread, depending on coherent structure size. It has been found in previous work [56] that ADCP's can suffer from near field boundary effects and this data setup has a very short blanking distance of only 10 cm, so the effect could be an artefact of the ADCP data, as would be suggested in the dissipation; i.e. being high in the bottom bins even when the velocities in the water column are low (Figure 7). Austin et al. [75] have noted a small inflection in the velocity measured in the closest range bin of a 3-beam Nortek Aquadopp in the benthic boundary layer of similar sites. This suggests that this could be a real effect, whereby the inflection is causing a change of sign in the $\overline{v'w'}$ Reynolds stress term and thus influencing P. Further work cross-referencing instruments such as ADV/Aquadopp/ADCP would tease out this uncertainty.

It has been suggested by Thomson et al. [7] that turbine power extraction efficiency may be a function of frequency and horizontal turbulent kinetic energy and that coherent eddies have been shown to produce the highest stresses in wind turbines, and as such these findings are of primary importance to the metrics to be used to understand the loading and power of tidal turbines. In the same work they finish with comments on the limitations of ADCP's due to the beam spread when utilising variance methods such as turbulent intensity and the need to further constrain the general structure of such eddies at tidal energy sites, suggesting the need for new instrumentation; this study suggests that this could be circumvented with metrics utilising the vertical beam. Moreover, such vertical ADCP beams could be placed in front of tidal energy turbines and the techniques illustrated here could assess the water/turbulent structure synoptically, with devices being powered accordingly for safe operation.

There are limitations in the applicability of the findings here, not least of which is the application of Taylor's "frozen field". Using this hypothesis for estimation of spatial information may preclude some of the complexity of the system. However, in order to circumvent this assumption one would need to collect both temporal and spatial data, which was not possible here, and could prove cost prohibitive for the tidal energy industry. Several previous studies [28, 15, 71] suggests that coherent structures are advected at speeds of $80 - 117\%$ of the free stream velocity thus, although not perfect, scaling the frequencies and periods with the mean flow speed is not such a reach.

Sample rates used to obtain frequencies for Taylor's "frozen field" are also worthy of consideration. The work of Thomson et al. [7] proves useful here whereby they suggest an appropriate sampling rate to ensure the signal is not aliased. By using only the vertical beam in these metrics and with the high sampling rate of 8Hz, while still using an appreciable depth range, this issue is circumvented. Horizontal fluctuations are most relevant to the tidal energy industry, but with isotropic turbulence one can obtain this information from the 'true' vertical component of an ADCP without the need for limitations of beam spread from the Janus beams. This could prove an issue with anisotropic turbulence, which is more prevalent at the larger scales, and this is an interesting area for further study.

5. Conclusion

To conclude, metrics from both single vertical beam techniques and that of the variance method utilising variance across beams have been computed.

Weaknesses have been identified in across beam techniques commonly used to understand turbulence at tidal energy sites, when coherent structures are present in the water column. TI and TKE P is obtained from the variance between Janus configuration beams on an ADCP. When coherent structures are prevalent covariance is present between beams, attributed to their lengthscales being of the same order as that of the beam spread, which means fundamental assumptions to this methods derivation are no longer valid.

However, metrics that are able to observe and characterise coherent structures in the water column using an off the shelf ADCP vertical beam have been identified; these are fast Fourier transforms (FFT) and a wavelet element model (WEM). As such techniques that use variance across beams in such environments should be replaced with vertical beam estimates using the metrics FFT and WEM.

6. Future Work

The coherent structures are thought to be created by interaction of the fluid with the seabed. Bathymetry data could elucidate to seabed structure influence on coherent structure size; dune spacing being apparent in the high resolution bathymetry data [51] providing an element lengthscale [28, 31].

This could prove extremely useful for the tidal energy industry when site scrutiny for turbine placement is considered.

Acknowledgements

This project was supported by Knowledge Economy Skills Scholarship (KESS 2, 80815/BUK2108) led by Bangor University on behalf of the Welsh higher education sector through funding from the Welsh European Funding Office (WEFO), the European Social Fund (ESF) and the company partner Nortek-AS, Norway. Thanks also goes out to the strong team of technicians at Bangor University that make this work possible; Peter Hughes and Aled Owen. We are very grateful to the anonymous reviewer for their valuable suggestions, which helped to improve the manuscript.

References

[1] CBC-News, Failed tidal turbine explained at symposium, 2011. URL: https://www.cbc.ca/news/canada/nova-scotia/failed-tidal-turbine-explained-at-symposium-1.1075510.

[2] F. Elasha, D. Mba, M. Togneri, I. Masters, J. A. Teixeira, A hybrid prognostic methodology for tidal turbine gearboxes, Renewable Energy 114 (2017) 1051–1061. doi:10.1016/j.renene.2017.07.093.

[3] Offshore-Energy, Muddy waters hold OpenHydro turbine broken at bay's bottom, 2018. URL: https://www.offshore-energy.biz/muddy-waters-hold-broken-openhydro-turbine-at-bays-bottom/.

[4] E. Osalusi, J. Side, R. Harris, Reynolds stress and turbulence estimates in bottom boundary layer of Fall of Warness, International Communications in Heat and Mass Transfer 36 (2009) 412–421. doi:10.1016/j.icheatmasstransfer.2009.02.004.

[5] R. O'Hara Murray, S. Ward, A. Goward-Brown, Conducting fieldwork in tidal stream sites, in: MASTS Annual Science Meeting, November, 2018, pp. 1–4.

[6] K. McCaffrey, B. Fox-Kemper, P. E. Hamlington, J. Thomson, Characterization of turbulence anisotropy, coherence, and intermittency at a prospective tidal energy site: Observational data analysis, Renewable Energy 76 (2015) 441–453. doi:10.1016/j.renene.2014.11.063.

[7] J. Thomson, B. Polagye, V. Durgesh, M. C. Richmond, Measurements of turbulence at two tidal energy sites in puget sound, WA, IEEE Journal of Oceanic Engineering 37 (2012) 363–374. doi:10.1109/JOE.2012.2191656.

[8] N. D. Kelley, R. M. Osgood, J. T. T. Bialasiewicz, A. Jakubowski, Using Time-Frequency and Wavelet Analysis to Assess Turbulence/Rotor Interactions, American Institute of Aeronautics and Astronautics 3 (2000) 121–134. doi:10.1002/we.33.

[9] N. D. Kelley, B. J. Jonkman, J. T. Bialasiewicz, G. N. Scott, L. S. Redmond, The Impact of Coherent Turbulence on Wind Turbine Aeroelastic Response and Its Simulation, American Wind Energy Association WindPower 2005 Conference and Exhibition (2005) 17.

[10] J. H. MacMahan, A. Reniers, W. Ashley, E. B. Thornton, Frequency-wavenumber velocity spectra, Taylor's hypothesis, and length scales in a natural gravel bed river, Water Resources Research 48 (2012). doi:10.1029/2011WR011709.

[11] A. Gyr, Discussion: Towards a better definition of the three types of sediment transport, Journal of Hydraulic Research 21 (1983) 389. doi:10.1080/00221688309499460.

[12] A. D. Heathershaw, "Bursting" phenomena in the sea, Nature 248 (1974) 394–395. doi:10.1038/248394a0.

[13] A. D. Heathershaw, Turbulent Structure of the Bottom Boundary-Layer in a Tidal Current, Geophysical Journal of the Royal Astronomical Society 58 (1979) 395–430.

[14] S. A. Talke, A. R. Horner-Devine, C. C. Chickadel, A. T. Jessup, Turbulent kinetic energy and coherent structures in a tidal river, Journal of Geophysical Research: Oceans 118 (2013) 6965–6981. doi:10.1002/2012JC008103.

[15] W. A. M. Nimmo Smith, S. A. Thorpe, A. Graham, Surface effects of bottom-generated turbulence in a shallow tidal sea, Nature 400 (1999) 251–254. doi:10.1038/22295.

[16] C. C. Chickadel, S. A. Talke, A. R. Horner-Devine, A. T. Jessup, Infrared-based measurements of velocity, turbulent kinetic energy, and dissipation at the water surface in a tidal river, IEEE Geoscience

and Remote Sensing Letters 8 (2011) 849–853. doi:10.1109/LGRS.2011.2125942.

[17] C. C. Chickadel, A. R. Horner-Devine, S. A. Talke, A. T. Jessup, Vertical boil propagation from a submerged estuarine sill, Geophysical Research Letters 36 (2009) 2–7. doi:10.1029/2009GL037278.

[18] K. F. Bowden, Measurements of Turbulence near the Sea Bed in a Tidal Current, Journal of Geophysical Research 67 (1962) 3181–3186.

[19] S. A. Thorpe, M. Green, J. H. Simpson, T. R. Osborn, W. A. M. Nimmo Smith, Boils and turbulence in a weakly stratified shallow tidal sea., Journal of Physical Oceanography 38 (2008) 1711–1730. doi:10.1175/2008JPO3931.1.

[20] A. N. Sukhodolov, V. I. Nikora, V. M. Katolikov, Flow dynamics in alluvial channels: The legacy of Kirill V. Grishanin, Journal of Hydraulic Research 49 (2011) 285–292. doi:10.1080/00221686.2011.567760.

[21] A. N. Sukhodolov, M. Thiele, H. Bungartz, C. Engelhardt, Turbulence structure in an ice-covered, sand-bed river, Water Resources Research 35 (1999) 889–894. doi:10.1029/1998WR900081.

[22] A. N. Sukhodolov, M. Thiele, H. Bungartz, Turbulence structure in a river reach with sand bed, water 34 (1998) 1317–1334.

[23] A. Tamburrino, J. S. Gulliver, Large flow structures in a turbulent open channel flow, Journal of Hydraulic Research/De Recherches Hydrauliques 37 (1999) 363–380. doi:10.1080/00221680109499810.

[24] H. Nakagawa, I. Nezu, Turbulence in Open Channel Flows, 1 ed., CRC Press, 1993.

[25] M. Thiébaut, J. F. Filipot, C. Maisondieu, G. Damblans, R. Duarte, E. Droniou, N. Chaplain, S. Guillou, J.-F. Filipota, C. Maisondieub, G. Damblansa, R. Duartea, E. Droniouc, N. Chaplaind, A comprehensive assessment of turbulence at a tidal-stream energy site influenced by wind-generated ocean waves, Energy 191 (2019). doi:10.1016/j.energy.2019.116550.

[26] M. Ikhennicheu, P. Druault, An experimental study of bathymetry influence on turbulence at a tidal stream site, in: EWTEC, 2017, pp. 1–10.

[27] R. J. Adrian, C. D. Meinhart, C. D. Tomkins, Vortex organization in the outer region of the turbulent boundary layer, Journal of Fluid Mechanics 422 (2000) S0022112000001580. doi:10.1017/S0022112000001580.

[28] R. J. Adrian, I. Marusic, Coherent structures in flow over hydraulic engineering surfaces, Journal of Hydraulic Research 50 (2012) 451–464. doi:10.1080/00221686.2012.729540.

[29] E. Corino, R. S. Brodkey, A visualization of the wall region in turbulent flow, Journal of Fluid Mechanics 37 (1969) 1–30.

[30] P. Ouro, T. Stoesser, Impact of Environmental Turbulence on the Performance and Loadings of a Tidal Stream Turbine, Flow, Turbulence and Combustion 102 (2019) 613–639. doi:10.1007/s10494-018-9975-6.

[31] M. Guala, C. D. Tomkins, K. T. Christensen, R. J. Adrian, Vortex organization in a turbulent boundary layer overlying sparse roughness elements, Journal of Hydraulic Research 50 (2012) 465–481. doi:10.1080/00221686.2012.729229.

[32] N. Hutchins, W. T. Hambleton, I. Marusic, Inclined cross-stream stereo particle image velocimetry measurements in turbulent boundary layers, Journal of Fluid Mechanics 541 (2005) 21–54. doi:10.1017/S0022112005005872.

[33] L. S. G. Kovasznay, The turbulent boundary layer, Ann. Rev. Fluid Mech. (1970).

[34] S. K. Robinson, A Review of Vortex Structures and Associated Coherent Motions in Turbulent Boundary Layers, Structure of Turbulence and Drag Reduction (1990) 23–50. doi:10.1007/978-3-642-50971-1_2.

[35] S. K. Robinson, Coherent Motions in the Turbulent Boundary Layer, Ann. Rev. Fluid Mech. (1991) 601–639.

[36] B. Johns, Some Consequences of an Inertia of Turbulence in a Tidal Estuary, Geophysical Journal International 18 (1969) 65–72.

[37] R. M. Horwitz, A. E. Hay, Turbulence dissipation rates from horizontal velocity profiles at mid-depth in fast tidal flows, Renewable Energy 114 (2017) 283–296. doi:10.1016/j.renene.2017.03.062.

[38] A. E. Hay, J. McMillan, R. Cheel, D. J. Schillinger, Turbulence and Drag in a High Reynolds Number Tidal Passage Targetted for In-Stream Tidal Power, Oceans 2013 San DIego (2013) 1–10.

[39] J. McMillan, A. E. Hay, R. G. Lueck, F. Wolk, Rates of Dissipation of Turbulent Kinetic Energy in a High Reynolds Number Tidal Channel, Journal of Atmospheric and Oceanic Technology 33 (2016) 817–837. doi:10.1175/JTECH-D-15-0167.1.

[40] P. J. Wiles, T. P. Rippeth, J. H. Simpson, P. J. Hendricks, A novel technique for measuring the rate of turbulent dissipation in the marine environment, Geophysical Research Letters 33 (2006). doi:ArtnL21608Doi10.1029/2006gl027050.

[41] R. K. Walter, N. J. Nidzieko, S. G. Monismith, Similarity scaling of turbulence spectra and cospectra in a shallow tidal flow, Journal of Geophysical Research: Oceans 116 (2011) 1–14. doi:10.1029/2011JC007144.

[42] R. Levy, D. Uminsky, A. Park, J. Calambokidis, A theory for the hydrodynamic origin of whale flukeprints, International Journal of Non-Linear Mechanics 46 (2011) 616–626. doi:10.1016/j.ijnonlinmec.2010.12.009.

[43] S. Salim, C. Pattiaratchi, R. Tinoco, G. Coco, Y. Hetzel, S. Wijeratne, R. Jayaratne, The influence of turbulent bursting on sediment resuspension under unidirectional currents, Earth Surface Dynamics 5 (2017) 399–415. doi:10.5194/esurf-5-399-2017.

[44] M. Gharib, A. Weigand, Experimental studies of vortex disconnection and connection at a free surface, Journal of Fluid Mechanics 321 (1996) 59–86. doi:10.1017/S0022112096007641.

[45] P. Mercier, M. Grondeau, S. Guillou, J. Thiébot, E. Poizot, Numerical Simulation of Large Turbulent Boils Generated by Sea Bottom Asperities, in: International Conference on Ocean Energy, Normandy University, University of Caen Normandy, ESIX, LUSAC, EA 4253, 2018.

[46] P. Mercier, M. Grondeau, S. Guillou, J. Thiébot, E. Poizot, Numerical study of the turbulent eddies generated by the seabed roughness. Case study at a tidal power site., Applied Ocean Research (2019).

[47] T. P. Rippeth, E. Williams, J. H. Simpson, Reynolds stress and turbulent energy production in a tidal channel, Journal of Physical Oceanography 32 (2002) 1242–1251.

[48] T. P. Rippeth, J. H. Simpson, E. Williams, M. E. Inall, Measurement of the rates of production and dissipation of turbulent kinetic energy in an energetic tidal flow: Red Wharf Bay revisited, Journal of Physical Oceanography 33 (2003) 1889–1901.

[49] B. D. Scannell, T. P. Rippeth, J. H. Simpson, J. A. Polton, J. E. Hopkins, Correcting surface wave bias in structure function estimates of turbulent kinetic energy dissipation rate, Journal of Atmospheric and Oceanic Technology 34 (2017) 2257–2273. doi:10.1175/JTECH-D-17-0059.1.

[50] R. Holt, Cloudbase Productions Limited, 2019.

[51] G. Walker-Springett, Bathymetry dataset, SEACAMS (2013), Bangor University. Personal Communication, 2020.

[52] Nortek-AS, Signature Integration Manual: N3015-007: V6 10/02/2017, 2017. doi:10.1002/ejoc.201200111. arXiv:arXiv:1011.1669v3.

[53] F. Bellard, FFMPEG, 2018.

[54] J. M. Lilly, Element analysis: a wavelet-based method for analyzing time-localized events in noisy time series, Proceedings of the Royal Society A: Mathematical, Physical and Engineering Sciences 473 (2017). doi:10.1098/rspa.2016.0776.

[55] M. Bakhoday-Paskyabi, I. Fer, J. Reuder, Correction to: Current and turbulence measurements at the FINO1 offshore wind energy site: analysis using 5-beam ADCPs (Ocean Dynamics, (2018), 68, 1, (109-130), 10.1007/s10236-017-1109-5), Ocean Dynamics 68 (2018) 157. doi:10.1007/s10236-017-1125-5.

[56] N. S. Lucas, J. H. Simpson, T. P. Rippeth, C. P. Old, Measuring turbulent dissipation using a tethered ADCP, Journal of Atmospheric and Oceanic Technology 31 (2014) 1826–1837. doi:10.1175/JTECH-D-13-00198.1.

[57] M. Guerra, J. Thomson, Turbulence Measurements From 5-Beam Acoustic Doppler Current Profilers, Journal of Atmospheric and Oceanic Technology 34 (2017) 1267–1284. doi:10.1175/JTECH-D-16-0148.1.

[58] A. Lohrmann, B. Hackett, L. P. Røed, High Resolution Measurements of Turbulence, Velocity and Stress Using a Pulse-to-Pulse Coherent Sonar, Journal of Atmospheric and Oceanic Technology 7 (1990) 19–37. doi:10.1175/1520-0426(1990)007<0019:HRMOTV>2.0.CO;2.

[59] M. T. Stacey, G. Monismith, J. R. Burau, Measurements of Reynolds stress profiles in unstratified tidal flow, Journal of Geophysical Research-Oceans 104 (1999) 933–949.

[60] G. I. Taylor, The spectrum of turbulence, Proceedings of the Royal Society of London A 164 (1938) 476–90.

[61] J. Thomson, B. Polagye, M. Richmond, V. Durgesh, Quantifying turbulence for tidal power applications, MTS/IEEE Seattle, OCEANS 2010 (2010). doi:10.1109/OCEANS.2010.5664600.

[62] J. M. Lilly, jLab: A data analysis package for Matlab, v. 1.6.6, 2019. URL: http://www.jmlilly.net/software.

[63] G. Katul, D. Poggi, D. Cava, J. Finnigan, The relative importance of ejections and sweeps to momentum transfer in the atmospheric boundary layer, Boundary-Layer Meteorology 120 (2006) 367–375. doi:10.1007/s10546-006-9064-6.

[64] C. J. Keylock, The visualization of turbulence data using a wavelet-based method, Earth Surface Processes and Landforms 32 (2007) 637–647.

[65] M. Mestres, M. Griñó, J. P. Sierra, C. Mösso, Analysis of the optimal deployment location for tidal energy converters in the mesotidal Ria de Vigo (NW Spain), Energy 115 (2016) 1179–1187. doi:10.1016/j.energy.2016.06.055.

[66] L. Myers, A. S. Bahaj, Simulated electrical power potential harnessed by

marine current turbine arrays in the Alderney Race, Renewable Energy 30 (2005) 1713–1731. doi:10.1016/j.renene.2005.02.008.

[67] M. J. Lewis, S. P. Neill, P. E. Robins, M. R. Hashemi, S. Ward, Characteristics of the velocity profile at tidal-stream energy sites, Renewable Energy 114 (2017) 258–272. doi:10.1016/j.renene.2017.03.096.

[68] A. Pérez-Ortiz, A. G. Borthwick, J. McNaughton, A. Avdis, Characterization of the tidal resource in Rathlin Sound, Renewable Energy 114 (2017) 229–243. doi:10.1016/j.renene.2017.04.026.

[69] R. O'Hara Murray, A. Gallego, A modelling study of the tidal stream resource of the Pentland Firth, Scotland, Renewable Energy 102 (2017) 326–340. doi:10.1016/j.renene.2016.10.053.

[70] S. P. Neill, J. R. Jordan, S. J. Couch, Impact of tidal energy converter (TEC) arrays on the dynamics of headland sand banks, Renewable Energy 37 (2012) 387–397. doi:10.1016/j.renene.2011.07.003.

[71] E. C. C. Steele, W. A. M. Nimmo Smith, A. Vlasenko, Direct measurement of hairpin-like vortices in the bottom boundary layer of the coastal ocean, Geophysical Research Letters 43 (2016) 1175–1183. doi:10.1002/2015GL067148.

[72] Y. Lu, R. G. Lueck, D. Huang, Turbulence Characteristics in a Tidal Channel, Journal of Physical Oceanography 30 (2000) 855–867.

[73] K. Korotenko, A. V. Sentchev, F. G. Schmitt, Effect of variable winds on current structure and Reynolds stresses in a tidal flow: Analysis of

experimental data in the eastern English Channel, Ocean Science 8 (2012) 1025–1040. doi:10.5194/os-8-1025-2012.

[74] H. Burchard, P. D. Craig, J. R. Gemmrich, H. van Haren, P. P. Mathieu, H. E. M. Meier, W. A. M. N. Smith, H. Prandke, T. P. Rippeth, E. D. Skyllingstad, W. D. Smyth, D. J. S. Welsh, H. W. Wijesekera, W. A. M. Nimmo Smith, H. Prandke, T. P. Rippeth, E. D. Skyllingstad, W. D. Smyth, D. J. S. Welsh, H. W. Wijesekera, Observational and numerical modeling methods for quantifying coastal ocean turbulence and mixing, Progress in Oceanography 76 (2008) 399–442. doi:DOI10.1016/j.pocean.2007.09.005.

[75] M. Austin, B. Lincoln, G. Walker-Springett, Non-equilibrium turbulent stresses and sediment transport in the benthic boundary layer of a shallow shelf environment influenced by flow obstruction, in: EGU General Meeting, Vienna, 2020.